Divergent Clinical and Immunologic Outcomes Based on *STK11* Co-mutation Status in Resectable *KRAS*-Mutant Lung Cancers Following Neoadjuvant Immune Checkpoint Blockade

Samuel Rosner[1,2], Sydney Connor[1,3], Khaled Sanber[1,4], Marianna Zahurak[1], Tianbei Zhang[1,3], Isha Gurumurthy[1,3], Zhen Zeng[1,3], Brad Presson[1,3], Dipika Singh[1,3], Roni Rayes[5], Lavanya Sivapalan[1], Gavin Pereira[1], Zhicheng Ji[6], Rohit Thummalapalli[7], Joshua E. Reuss[1,8], Stephen R. Broderick[1], David R. Jones[7], Julie S. Deutsch[3,9], Tricia R. Cottrell[10], Jamie E. Chaft[7,11], Jonathan Spicer[5], Janis Taube[1,3,9], Valsamo Anagnostou[1], Julie R. Brahmer[1], Drew M. Pardoll[1,3], Hongkai Ji[12], Patrick M. Forde[1], Kristen A. Marrone[1], and Kellie N. Smith[1,3]

ABSTRACT

Purpose: Co-mutations of the *Kirsten rat sarcoma virus* (*KRAS*) and *serine/threonine kinase 11* (*STK11*) genes in advanced non–small cell lung cancer (NSCLC) are associated with immune checkpoint blockade (ICB) resistance. Although neoadjuvant chemoimmunotherapy is now a standard-of-care treatment for resectable NSCLC, the clinical and immunologic impacts of *KRAS* and *STK11* co-mutations in this setting are unknown.

Experimental Design: We evaluated and compared recurrence-free survival of resectable *KRAS*-mutated NSCLC tumors, with or without co-occurring *STK11* mutations, treated with neoadjuvant ICB. Single-cell transcriptomics was performed on tumor-infiltrating T cells from seven $KRAS^{mut}/STK11^{wt}$ tumors and six *KRAS* and *STK11* co-mutated ($KRAS^{mut}/STK11^{mut}$) tumors.

Results: Relative to $KRAS^{mut}/STK11^{wt}$ tumors, $KRAS^{mut}/STK11^{mut}$ exhibited significantly higher recurrence risk. Single-cell transcriptomics showed enhanced oxidative phosphorylation with evidence of decreased prostaglandin E2 signaling and increased IL-2 signaling in $CD8^+$ tumor-infiltrating lymphocytes (TIL) from $KRAS^{mut}/STK11^{mut}$ tumors, a finding that was mirrored in $KRAS^{wt}$ tumors that relapsed. TILs from $KRAS^{mut}/STK11^{mut}$ tumors expressed high levels of molecules associated with tumor residence, including CD39 and ZNF683 (HOBIT).

Conclusions: These divergent T-cell transcriptional fates suggest that T-cell maintenance and residence may be detrimental to anti-tumor immunity in the context of neoadjuvant ICB for resectable NSCLC, regardless of *KRAS* mutation status. Our work provides a basis for future investigations into the mechanisms underpinning prostaglandin E2 signaling and IL-2 signaling as they relate to T-cell immunity to cancer and to divergent clinical outcomes in $KRAS^{mut}/STK11^{mut}$ NSCLC treated with neoadjuvant ICB.

Introduction

Neoadjuvant or perioperative chemoimmunotherapy is standard of care for the management of resectable non–small cell lung cancer (NSCLC; refs. 1–3). Response to neoadjuvant immune checkpoint blockade (ICB) can be assessed at the time of resection by quantifying the pathologic regression of tumor and using standardized thresholds for pathologic complete response (pCR) and major pathologic response (MPR; ref. 4), which have been associated with improved event-free survival in lung cancer (5). Further investigation and refinement of biomarkers predictive of response and clinical outcomes with neoadjuvant ICB are needed to help guide subsequent treatment postoperatively.

The *Kirsten rat sarcoma virus* (*KRAS*) gene has activated mutations in 40% of NSCLC, making it the most commonly mutated oncogenic driver gene in this cancer. Tumors with these mutations have heterogeneous response patterns to anti–PD-1–directed regimens in the advanced disease setting (6), despite an association with

[1]Department of Oncology, Johns Hopkins Sidney Kimmel Comprehensive Cancer Center, Baltimore, Maryland. [2]University of Maryland Marlene and Stewart Greenebaum Comprehensive Cancer Center, Baltimore, Maryland. [3]Bloomberg~Kimmel Institute for Cancer Immunotherapy, Johns Hopkins University, Baltimore, Maryland. [4]Department of Thoracic, Head and Neck Medical Oncology, MD Anderson Comprehensive Cancer Center, Houston, Texas. [5]Division of Thoracic Surgery, McGill University Health Center, Montreal, Canada. [6]Department of Biostatistics and Bioinformatics, Duke University School of Medicine, Durham, North Carolina. [7]Thoracic Oncology Service, Memorial Sloan Kettering Cancer Center, New York, New York. [8]Department of Oncology, Georgetown Lombardi Comprehensive Cancer Center, Washington, District of Columbia. [9]Department of Dermatology, Johns Hopkins School of Medicine, Baltimore, Maryland. [10]Department of Pathology and Molecular Medicine, Queens Cancer Research Institute, Kingston, Canada. [11]Weill Cornell Medical College, School of Medicine, New York, New York. [12]Department of Biostatistics, Johns Hopkins Bloomberg School of Public Health, Baltimore, Maryland.

S. Rosner and S. Connor contributed equally as co-first authors.

K.A. Marrone and K.N. Smith contributed equally as co-last authors.

Corresponding Author: Kellie N. Smith, Bloomberg-Kimmel Institute for Cancer Immunotherapy, Johns Hopkins Medicine, CRB1, Room 4M51 1650 Orleans Street, Baltimore, MD 21287. E-mail: kellie@jhmi.edu

Clin Cancer Res 2025;31:339–51

doi: 10.1158/1078-0432.CCR-24-2983

Translational Relevance

This report represents an early, in-depth clinical and immunologic analysis of resectable *KRAS*-mutant NSCLC treated with neoadjuvant ICB. We show a preliminary signal of divergent clinical outcomes based on the *STK11* co-mutation status as well as distinctive phenotypic and metabolic profiles of $CD8^+$ TILs that may underlie these clinical outcomes.

smoke exposure, positive PD-L1 expression, and high tumor mutational burden (TMB) (7), which are all features that have been independently associated with a favorable response to ICB (8, 9). This difference in outcomes seems to be partly associated with the presence or absence of key co-occurring alterations (10), such as *serine/threonine kinase 11* (*STK11*) and Kelch-like erythroid-derived cap'n'collar homolog (ECH)-associated protein 1 (*KEAP1*). Bulk RNA sequencing (RNA-seq) suggested that *KRAS* and *STK11* co-mutated ($KRAS^{mut}/STK11^{mut}$) tumors have alterations in their tumor immune microenvironment (TME) relative to $KRAS^{mut}/STK11^{wt}$ NSCLC, which could contribute to the differential response patterns to PD-1 therapy. However, this association has yet to be evaluated in the resectable disease setting.

Our group has previously demonstrated differential transcriptional features of tumor-reactive $CD8^+$ tumor-infiltrating lymphocytes (TIL) and highlighted transcriptional differences in tumor-reactive $CD8^+$ TILs based on the extent of pathologic response to neoadjuvant PD-1 blockade in resectable NSCLC (11). However, characterization of TIL function based on clinically relevant genomic subgroups as it relates to clinical outcome following neoadjuvant PD-1 therapy has not been previously described.

In order to glean potential effects of the $KRAS^{mut}/STK11^{mut}$ co-mutation on T-cell transcriptional programs within the tumor, we performed an integrated clinical and single-cell RNA-seq analysis of TILs from patients with resectable stage I–III *KRAS*-mutant NSCLC enrolled in a phase I/II, multiarm clinical trial (NCT02259621) treated with neoadjuvant ICB-based therapies. Among patients with *KRAS*-mutant disease, despite relative equivalent rates of MPR regardless of the co-mutation status with *STK11*, we noted increased recurrence risk in patients with $KRAS^{mut}/STK11^{mut}$ disease. Furthermore, single-cell transcriptional analysis of tumor-infiltrating $CD8^+$ TILs from available resection specimens revealed distinctive transcriptional profiles based on *STK11* co-mutation status. Increased expression of genes encoding canonical cytolytic effector molecules was accompanied by increased expression of T-cell checkpoints and molecules associated with tissue residence in $CD8^+$ TILs from $KRAS^{mut}/STK11^{mut}$ tumors, whereas $CD8^+$ TILs from $KRAS^{mut}/STK11^{wt}$ tumors exhibited features associated with proliferative potential and, surprisingly, demonstrated expression profiles consistent with prostaglandin E2 (PGE2) signaling and downregulation of IL-2 signaling. These findings suggest that *STK11* mutations in $KRAS^{mut}$ lung cancers may negatively impact clinical outcomes to neoadjuvant ICB via promotion of chronic T-cell stimulation and tissue residence.

Materials and Methods

Patient selection and eligibility

This study was performed in accordance with the Declaration of Helsinki and was approved by the Johns Hopkins University Institutional Review Board and the US Department of Health and Human Services. This was a retrospective, exploratory analysis of patients enrolled on a multicohort, multi-institution, phase I/II clinical trial (NCT02259621) conducted at Johns Hopkins University, Memorial Sloan Kettering Cancer Center, and McGill University. Eligible patients, including those of ≥18 years of age, with untreated, resectable stage I (>4 cm)–III NSCLC, per seventh edition American Joint Committee on Cancer, were sequentially assigned to three different neoadjuvant treatment regimens. Additional eligibility criteria have been previously described (12–14).

Treatment procedures

Enrolled patients were assigned to three different neoadjuvant ICB-based treatment regimens before undergoing preplanned definitive resection. Cohort 1 received preoperative nivolumab monotherapy followed by preplanned resection within 24 days from the last dose of systemic therapy. Of note, an initial nivolumab monotherapy cohort ($n = 21$) received two preoperative cycles of nivolumab (3 mg/kg every 2 weeks) followed by a later expansion of 16 patients who received three preoperative cycles of nivolumab (240 mg every 2 weeks). Cohort 2 received nivolumab (3 mg/kg) together with ipilimumab 1 mg/kg intravenously approximately 6 weeks prior to planned resection, followed by two additional doses of nivolumab 3 mg/kg given at approximately 4 and 2 weeks preoperatively. Cohort 3 received nivolumab (360 mg every 3 weeks) combined with carboplatin (AUC 5 or 6 every 3 weeks) and paclitaxel (175–200 mg/m^2 every 3 weeks) for three preoperative cycles before undergoing preplanned surgical resection within 6 weeks of completing systemic therapy (Supplementary Fig. S2A). Standard-of-care adjuvant therapy options, including postoperative radiotherapy and/or chemotherapy, were allowed and offered per the provider's discretion.

Clinical endpoints and biomarkers

Primary endpoints for cohorts 1 and 2 were safety and feasibility. The primary endpoint for cohort 3 was the rate of pCR for patients who underwent definitive resection. This secondary analysis aimed to explore pathologic, clinical, and immunologic responses among key genomic subgroups within this multicohort trial that were treated with various ICB-based neoadjuvant regimens (Supplementary Fig. S2B).

Key pathologic endpoints in this analysis were the rate of institutionally assessed pCR and MPR, defined as 0% and ≤10% residual viable tumor, respectively, for all patients who underwent definitive resection (4). A key clinical endpoint included relapse-free survival (RFS) for patients who underwent definitive resection, measured from the time of surgery to the date of recurrence or last follow-up. Overall survival (OS) was measured from the date of first neoadjuvant treatment to the date of death or last follow-up for all treated patients. Definitive resection was defined as completed surgical resection without positive margins (R0 resection).

Somatic tumor genomic alterations were reported from all available pretreatment specimens using either targeted gene panels or whole-exome sequencing. For the purposes of this analysis, patients with *KRAS*, *EGFR*, *MET* exon 14 skipping, $BRAF^{V600E}$, *ALK*, *HER2*, *ROS1*, *RET*, or *NTRK* alterations were categorized as having oncogene-driven NSCLC. Additional prognostic genomic markers, including *STK11*, *KEAP1*, and *TP53*, were recorded. An exploratory analysis was performed to evaluate associations of key genomic subgroups and pathologic or clinical outcomes.

IHC was performed for pretreatment tumor PD-L1 evaluation. PD-L1 staining was performed on formalin-fixed, paraffin-embedded tissue sections using the Dako PD-L1 IHC 28–8 pharmDx assay. Samples were considered PD-L1$^+$ if ≥1% of tumor cells showed membranous PD-L1 expression.

Statistical analysis of clinical data

Proportions are reported with exact 95% binomial confidence intervals (CI). Binomial probabilities are compared using the χ^2 or Fisher exact test. The Freeman–Halton extension of the Fisher exact probability test was utilized for a 2 × 3 contingency table when evaluating the impact of treatment type on pathologic response. Factors associated with pCR and MPR were selected based on univariate and multivariate logistic regression analyses. OS, RFS, and median follow-up are reported using the Kaplan–Meier and reverse Kaplan–Meier methods. Comparisons are made using the Cox proportional hazards regression model. All *P* values reported are two-sided, and the significance level was set at 0.05 for all analyses. Statistical analyses were performed using R version 4.1.3.

Sample processing

After acquiring written informed consent, peripheral blood mononuclear cells and resected tissues were obtained from patients undergoing surgical resection. Tissues were enzymatically digested and viably frozen. If available, normal adjacent lung, lymph nodes, and metastases were also digested and frozen down after surgery.

Single-cell T-cell receptor sequencing/RNA-seq

These methods have been published in detail previously (11). In brief, cryobanked T cells were thawed and washed twice with pre-warmed RPMI with 20% FBS and gentamicin. Cells were resuspended in PBS and incubated with Fc block for 15 minutes on ice. Surface staining with antibody against CD3 (BV421, clone SK7; RRID: AB_2870486 or APC, clone SK7; RRID: AB_2833003) was performed for 30 minutes on ice. Viability was stained using LIVE/DEAD Fixable Near-IR (Thermo Fisher Scientific) or propidium iodide according to the manufacturer's protocol. After staining, highly viable CD3$^+$ T cells were sorted into 0.04% BSA in PBS using a BD FACSAria II cell sorter or MoFlo XDP sorter. Sorted cells were manually counted using a hemocytometer and prepared at the desired cell concentration (1,000 cells/μL) when possible. The Single-Cell 5′ V(D)J and 5′ digital gene expression (DGE) kits (10× Genomics) were used to capture immune repertoire information and gene expression from the same cell in an emulsion-based protocol at the single-cell level. Cells and barcoded gel beads were partitioned into nanoliter-scale droplets using the 10× Genomics Chromium platform to partition up to 10,000 cells per sample followed by RNA capture and cell-barcoded cDNA synthesis using the manufacturer's standard protocols. Libraries were generated and sequenced on an Illumina NovaSeq instrument using 2 × 150-bp paired end sequencing. The 5′ VDJ libraries were sequenced to a depth of ~5,000 reads per cell, for a total of 5 million to 25 million reads. The 5′ DGE libraries were sequenced to a target depth of ~50,000 reads per cell.

Single-cell data processing and quality control

Cell Ranger v7.1.0 was used to demultiplex the FASTQ reads, align them to the GRCh38 human transcriptome, and extract their cell and unique molecular identifier barcodes. The output of this pipeline is a DGE matrix for each sample, which records the number of unique molecular identifiers for each gene that are associated with each cell barcode. The quality of cells was then assessed based on (i) the number of genes detected per cell and (ii) the proportion of mitochondrial gene/ribosomal gene counts. Low-quality cells were filtered if the number of detected genes was below 250 or above 3× the median absolute deviation away from the median gene number of all cells. Cells were filtered out if the proportion of mitochondrial gene counts was higher than 10% or the proportion of ribosomal genes was less than 10%. A table outlining the cells that passed these quality control cutoffs at both patient and sample levels can be found in Supplementary Table S3. For single-cell VDJ sequencing, only cells with full-length sequences were retained. Dissociation/stress-associated genes, mitochondrial genes (annotated with the prefix "MT-"), high-abundance long intergenic non-coding RNA (lincRNA) genes, genes linked with poorly supported transcriptional models (annotated with the prefix "RP-"), and T-cell receptor (TCR; TR) genes (TRA/TRB/TRD/TRG, to avoid clonotype bias) were removed from further analysis. In addition, genes that were expressed in less than five cells were excluded.

Single-cell data integration and clustering

Seurat (5.0.1) was used to normalize the raw count data, identify highly variable features and scale features, and integrate samples. Principal component analysis (PCA) was performed based on the 3,000 most variable features identified using the vst method implemented in Seurat. Gene features associated with type I IFN response, immunoglobulin genes, and specific mitochondrion-related genes were excluded from clustering to avoid cell subsets driven by the above genes. Dimension reduction was done using the Run Uniform Manifold Approximation and Projection function. Cell markers were identified using a two-sided Wilcoxon rank-sum test. Genes with adjusted $P < 0.05$ were retained. Clusters were labeled based on the expression of the top differential gene in each cluster as well as canonical immune cell markers. Global clustering on all CD3 T cells and refined clustering on CD8 T cells were performed using the same procedure. A stringent *CD8A* cutoff of 1.5 was set based upon expression of each T-cell subtype within the CD3 clustering; this was done to ensure that the refined clustering only included *bona fide* CD8 TILs.

Single-cell subset pseudobulk gene expression analysis

PCA was performed on a standardized pseudobulk gene expression profile, in which each feature was standardized to have a mean of zero and unit variance. In the global CD3 PCA, we aggregated read counts across cells within each sample to produce a pseudobulk expression profile and normalized these pseudobulk expression profiles across samples by library size. The ComBat function in the sva R package was applied to address potential batch effects on the normalized pseudobulk profile. Highly variable genes (HVG) were selected for each cell cluster by fitting a locally weighted scatterplot smoothing regression of SD against the mean for each gene and identifying genes with positive residuals. For each sample, all cell clusters were then concatenated by retaining each cluster's HVGs to construct a concatenated gene expression vector consisting of all highly variable features identified from different cell clusters. Each element in this vector represents the pseudobulk expression of an HVG in a cell cluster. Samples were embedded into the PCA space based on these concatenated gene expression vectors. Canonical correlation between the first two principal components (PC1 and PC2) and a covariate of interest (*STK11* co-mutation status or recurrence status) was calculated. The permutation test was used to assess the significance by randomly permuting the sample

labels 10,000 times. The *P* value was calculated as the number of permutations of 10,000 permutations that produce a likelihood ratio larger than the observed one, without correction for multiple comparisons.

Differential gene expression profiling

The gene expression read counts were adjusted by library size. SAVER was used to impute dropouts by borrowing information across similar genes and cells. A linear mixed-effect model was constructed to identify genes that are significantly differential based on co-mutation status ($KRAS^{mut}/STK11^{mut}$ vs. $KRAS^{mut}/STK11^{wt}$) among $CD8^+$ TILs, using the raisin R package. The Benjamini-Hochberg procedure was used to adjust the *P* values for multiple testing, and the statistical significance was determined using a cutoff of FDR <0.05. Individual genes were queried within the imputation gene matrix based upon these findings.

Gene score generation

To characterize the phenotype of NSCLC TILs, the checkpoints, *CTLA4*, *PDCD1*, *LAG3*, *HAVCR2*, *TIGIT*, and *ENTPD1*, were used to compute the T-cell checkpoint score (11). The cytotoxicity score [*perforin 1* (*PRF1*), *IFNG*, *FASLG*, *GZMA*, *GZMB*, *GZMH*, *GZMK*, and *GNLY*] and memory score (*IL-7R*, *SELL*, *CCR7*, *CD28*, and *TCF7*) were also previously published (15). In addition, gene sets previously described within Fernández-García and colleagues (16) for aerobic glycolysis and oxidative phosphorylation (OXPHOS) were converted from mouse to human. Additionally, we utilized the Reactome pathways taken from MSigDB (https://www.gsea-msigdb.org/gsea/msigdb/; extracted from the C2 collection). The IL-2 signaling score was extracted from Reactome under the "REACTOME_INTERLEUKIN_2_SIGNALING" name. SAVER-imputed expression values were used for these scores. Each score is equal to the mean expression value of all the genes within each respective gene set for each cell. The ratio of OXPHOS to aerobic glycolysis was calculated by dividing the OXPHOS score by the aerobic glycolysis score for each cell.

Data availability

All processed and deidentified single-cell data from the neoadjuvant-treated human samples are available in the Gene Expression Omnibus with accession number GSE280232. All data needed to evaluate the conclusions are present in the article or the Supplementary Materials. Additional information or data can be obtained by contacting the corresponding authors. Scripts to reproduce the analyses used in this study are available at https://github.com/BKI-immuno/neoantigen-specific-T-cells-NSCLC.

Results

Clinical features and outcomes of resectable $KRAS^{mut}$ lung cancers treated with neoadjuvant ICB

Our clinical study cohort included 61 patients who received neoadjuvant ICB-based therapies as part of a phase I/II, multiarm, clinical trial (NCT02259621). Patients received either nivolumab monotherapy ($n = 37$), nivolumab plus ipilimumab ($n = 9$), or nivolumab with platinum doublet chemotherapy ($n = 15$) prior to surgical resection (Supplementary Fig. S1A). The median age at study enrollment was 67 years, and 55 patients (90.2%) had current or prior smoking history. Forty-three tumors were of nonsquamous histology (71%). Nearly half of patients ($n = 29$) had stage III disease. A positive PD-L1 expression level by IHC was noted in 48% of patients on pretreatment specimens, whereas 16 patient tumor samples did not have available baseline PD-L1 results.

Pretreatment genomic sequencing data were available for 52 patients (**Table 1**; Supplementary Table S1; Supplementary Fig. S1B), 21 (40.4%) of whom were found to harbor a mutation in the *KRAS* gene, which is consistent with prior reports of the frequency of *KRAS* mutations in metastatic lung cancers (17). In total, there were 14 tumors that harbored a *KRAS* mutation without detection of an *STK11* co-mutation ($KRAS^{mut}/STK11^{wt}$) and seven tumors with mutations in both *KRAS* and *STK11* ($KRAS^{mut}/STK11^{mut}$). Further demographic and genomic details for the full cohort ($n = 61$) and the subset of *KRAS*-mutant patients ($n = 21$) are noted in **Table 1** and Supplementary Table S1.

The rates of pCR and MPR for $KRAS^{wt}$ tumors were 14% and 45%, respectively, with a definitive resection rate of 93.5%. For the $KRAS^{mut}$ cohort ($n = 21$), the rates of pCR and MPR were 6% and 22%, respectively. There was a trend toward a higher rate of MPR in $KRAS^{wt}$ than $KRAS^{mut}$ tumors; however, this did not reach statistical significance (Supplementary Fig. S2A; 22% vs. 45%; $P = 0.135$). In total, 18 $KRAS^{mut}$ tumors were surgically resected (definitive resection rate of 85.7%). The three patients who did not undergo surgical resection were found to have primary disease progression prior to or at surgery, leading to termination of attempted definitive resection, and were therefore excluded from our formal calculation of pathologic response. In this limited sized cohort, there was no statistical difference in the rate of MPR between the $STK11^{wt}$ (25%) and $STK11^{mut}$ (17%) $KRAS^{mut}$ tumors that were surgically resected (**Fig. 1A**; $P = 1.0$). However, it is worth noting that of the patients with primary progression of their $KRAS^{mut}$ disease, two of these tumors were *KEAP*1 mutated and the third harbored an *STK11* mutation (Supplementary Table S1), suggesting that these co-mutations may indeed mark aggressive primary tumors that are resistant to neoadjuvant ICB and have high metastatic potential. In alignment with this observation, using 50% residual viable tumor as an alternative cutoff value for meaningful pathologic response—which has been utilized in other solid tumor malignancies (18)—there is a trend toward weaker pathologic response in the $KRAS^{mut}/STK11^{mut}$ (17%) versus the $KRAS^{mut}/STK11^{wt}$ (50%) subcohorts (Supplementary Fig. S2B; $P = 0.32$). A subsequent assessment of pathologic response, including patients with primary progression, revealed pCR rates of 13%, and 5% for our $KRAS^{wt}$ ($n = 31$) and $KRAS^{mut}$ ($n = 21$) cohorts, respectively (Supplementary Fig. S2C; $P = 0.64$). Examining the impact of treatment type on pathologic response, there was no significant differences noted in MPR or pCR across resected patients in our full cohort (MPR, $P = 0.71$; pCR $P = 0.25$) or $KRAS^{mut}$ cohort (MPR, $P = 0.62$; pCR, $P = 0.17$; Supplementary Table S2).

At the time of this analysis, the median follow-up time was 30.4 months (95% CI, 15.5–59.4) for the 21 patients with $KRAS^{mut}$ disease. Of the 14 $KRAS^{mut}/STK11^{wt}$ tumors, 2 harbored co-mutations with *KEAP1*. Both of these patients experienced primary progression of their disease and died within 1 year of their surgery (**Fig. 1C**). There were two additional recurrence events in the $KRAS^{mut}/STK11^{wt}$ subcohort, both intracranial and occurring >12 months from surgery (14.5 and 27 months, respectively). In comparison, for the seven patients who had $KRAS^{mut}/STK11^{mut}$ disease, one patient had primary progression precluding surgery, and four had recurrence of their disease (two intracranial and two intrathoracic recurrences). The time to recurrence for these four patients was 1.9, 6.5, 14.0, and 16.0 months from surgery. Of

Table 1. Summary of demographic data, neoadjuvant treatment, and surgical outcomes for all subjects ($n = 61$) and patients with *KRAS*-mutant disease ($n = 21$).

Characteristic	All patients ($n = 61$)	*KRAS*-mutant cohort ($n = 21$)
Median age at enrollment—years (range)	67 (44–84)	62 (50–78)
Female—number (%)	29 (47.5%)	13 (61.9%)
Current/former smoker—number (%)	55 (90.2%)	21 (100%)
Never smoker—number (%)	6 (9.8%)	0 (0%)
Histology—number (%)		
Adenocarcinoma	40 (65.6%)	19 (90.5%)
Squamous cell carcinoma	18 (29.5%)	2 (9.5%)
Other histology[a]	3 (4.9%)	0 (0%)
Stage[b]—number (%)		
I	6 (9.8%)	1 (4.8%)
II	26 (42.6%)	11 (52.4%)
III	29 (47.5%)	9 (42.9%)
Treatment type—number (%)		
Nivo monotherapy	37 (60.7%)	9 (42.9%)
Nivo plus ipilimumab	9 (14.8%)	5 (23.8%)
Nivo plus chemotherapy	15 (24.6%)	7 (33.3%)
Surgical outcomes—number (%)		
Underwent definitive resection	56 (91.8%)	18 (85.7%)
Primary progression of disease	5 (8.2%)	3 (14.3%)
Adjuvant therapy—number (%)		
Yes	18 (29.5%)	7 (33.3%)
No	43 (70.5%)	14 (66.7%
Pretreatment PD-L1 expression[c]—number (%)		
PD-L1 <1%	22 (36.1%)	8 (38.1%)
PD-L1 ≥1%	29 (47.5%)	9 (42.6%)
Not available	10 (16.4%)	4 (19.1%)
Baseline genomic sequencing available—number (%) $N = 52$[d]		
KRAS^{G12c}	6 (11.5%)	6 (28.6%)
KRAS non-G12c[e]	15 (28.9%)	15 (71.4%)
STK11 mutant	10 (19.2%)	7 (33.3%)
KEAP1 mutant	5 (9.6%)	2 (9.5%)
TP53 mutant	30 (57.7%)	11 (52.4%)

Abbreviation: Nivo, nivolumab.
[a]Other histologic diagnoses included pleomorphic and adenosquamous carcinomas.
[b]Clinical staging was per American Joint Committee on Cancer tumor–node–metastases seventh edition.
[c]On the basis of pretreatment tumor PD-L1 expression (TPS <1% vs. ≥1%). There were 10 patients whose pretreatment PD-L1 assessment was not available.
[d]Fifty-two subjects with available baseline genomic sequencing.
[e]*KRAS* non-G12c mutations in this analysis included *KRAS*^{G12V}, *KRAS*^{Q61H}, *KRAS*^{G12D}, *KRAS*^{G12A}, *KRAS*^{G12F}, and *KRAS*^{G13C}.

note, there was one *KRAS*^{mut}/*STK11*^{mut} tumor with PD-L1 <1% expression and co-occurring *BAP1* alteration with an MPR after neoadjuvant chemoimmunotherapy. Despite this significant pathologic regression of their tumor, this patient had recurrence as stated above (14 months after surgery).

For these 21 patients, the 5-year RFS and OS rates were 58% and 85%, respectively (Supplementary Figs. S1D and S2D). Recurrence risk was comparable regardless of *KRAS* mutation status (HR = 1.0; 95% CI, 0.37–2.71; $P = 0.993$; **Fig. 1D**), type of *KRAS* mutation (G12C vs. non-G12C; HR 2.74; 95% CI, 0.55–13.71; $P = 0.22$, Supplementary Fig. S2E), or *TP53* co-mutation status (HR = 0.9; 95% CI, 0.18–4.55; $P = 0.897$, Supplementary Fig. S2F). However, a divergence in recurrence outcomes was noted within the *KRAS*^{mut} subcohort, with a significantly higher risk of recurrence in the presence of *STK11* co-mutation (HR = 7.09; 95% CI, 1.25–40.1; $P = 0.027$; **Fig. 1E**), with a median RFS of 14.03 months for *KRAS*^{mut}/*STK11*^{mut} tumors, and the median RFS for *KRAS*^{mut}/*STK11*^{wt} tumors not reached. A similar signal was also noted based on *STK11* mutation status regardless of *KRAS* mutation status (HR = 3.3; 95% CI, 1.11–9.76; $P = 0.031$; Supplementary Fig. S2G); however, it is worth noting that only two of these tumors were *KRAS*^{wt} (Supplementary Table S1).

CD8^{+} TILs from KRAS^{mut}/STK11^{mut} tumors are transcriptionally distinct

We previously detected a high frequency of neoantigen-specific TILs in one of these *KRAS*^{mut}/*STK11*^{mut} tumors that did not achieve MPR (patient MD043-011; ref. 11). Although anecdotal, this finding demonstrated that tumor-reactive TILs can be generated in patients with ICB-resistant *KRAS*^{mut}/*STK11*^{mut} lung tumors. We therefore hypothesized that it is the quality, rather than the quantity, of the TILs that permits earlier relapse in these patients. To therefore better understand the immunologic underpinnings of the increased risk of recurrence in patients with *KRAS*^{mut}/*STK11*^{mut} tumors, we performed single-cell TCR sequencing (TCR-seq)/RNA-seq on biospecimens from six patients with *KRAS*^{mut}/*STK11*^{mut} disease and seven patients with *KRAS*^{mut}/*STK11*^{wt} disease treated with neoadjuvant ICB (**Fig. 2A**). All *KRAS*^{mut}/*STK11*^{mut} tumors were confirmed to have functionally and/or clinically relevant *STK11* mutations (Supplementary Table S1; ref. 19). Treatment

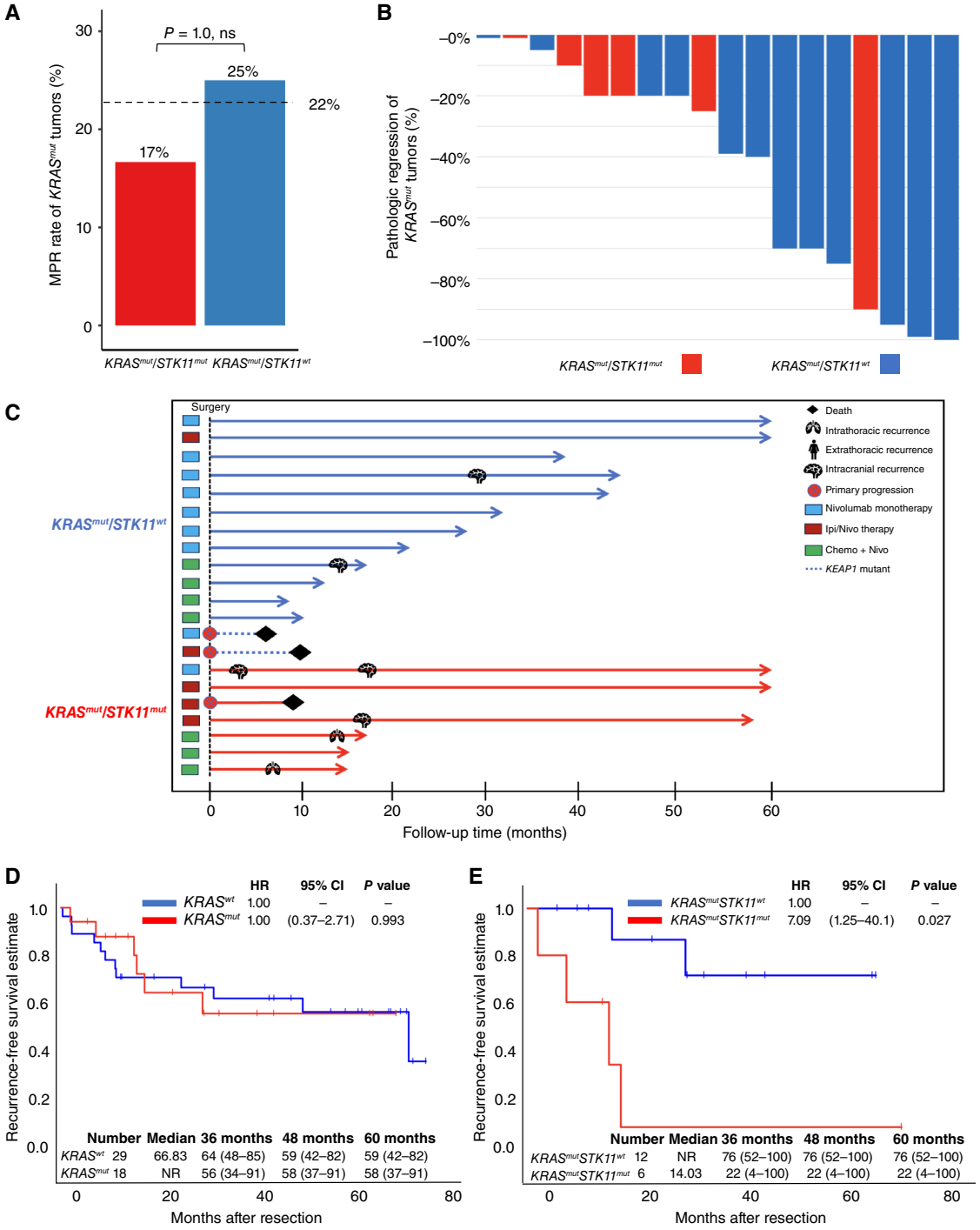

Figure 1.

Pathologic and clinical outcomes of patients with *KRAS*-mutant NSCLC treated with neoadjuvant ICB. **A,** Bar graph presenting the MPR rate for patients with *KRAS*-mutant disease, based on co-mutation status with *STK11*. The MPR rate for the whole *KRAS*-mutant cohort is also included as a dotted line for reference and comparison. **B,** Waterfall plot depicting percent pathologic regression of primary tumor for our *KRAS*-mutant cohort that underwent definitive resection, determined by baseline genomic sequencing prior to neoadjuvant ICB. Therefore, two patients with $KRAS^{mut}/STK11^{wt}$ disease and one patient with $KRAS^{mut}/STK11^{mut}$ disease were not included as they had primary progression precluding definitive resection. **C,** Swimmer plot summarizing treatment type and clinical outcomes for all patients with *KRAS*-mutant disease divided by the presence or absence of co-occurring *STK11* mutation. Patients with primary progression of disease are denoted in this figure, as well as *KEAP1* mutation status. Ipi, ipilimumab; Nivo, nivolumab. **D,** Kaplan–Meier curves depicting recurrence-free survival for patients based on *KRAS* mutation status. **E,** Kaplan–Meier curves depicting recurrence-free survival for the *KRAS*-mutant cohort based on co-mutation status with *STK11*.

type was evenly distributed among these 13 patients, with 4 receiving nivolumab monotherapy, 4 receiving nivolumab and ipilimumab, and 5 receiving nivolumab plus chemotherapy. Single-cell TCR-seq/RNA-seq was reported previously for *KRAS*^{mut}/*STK11*^{mut} patient MD043-011 who was treated with neoadjuvant nivolumab monotherapy (11).

CD8$^+$ T-cell clustering was performed on tumor ($n = 13$) and adjacent normal lung ($n = 8$). Following rigorous quality control to remove low-quality cells, transcriptomic profiles were defined for 92,525 CD8$^+$ T cells that formed 14 unique clusters (**Fig. 2A**; Supplementary Table S3). Clusters were annotated based on previously defined T-cell states. The top cluster defining genes and localization of expression within gene overlays were both used in cell-type assignment (**Fig. 2C**). The tissue-resident memory (TRM) subsets were assigned based on high expression of *ZNF683* (HOBIT) and *ITGAE* (CD103; **Fig. 2B**). These TRM clusters also had notable expression of *EOMES* and several granzymes and intermediate expression of *KLRG1* and *CXCR3*. Additionally, we observed a terminally dysfunctional TRM subset co-expressing multiple T-cell checkpoints, *CD39*, and *CXCL13* (**Fig. 2B**), all of which we had shown previously to be upregulated in validated neoantigen-specific CD8 T cells (11). Interestingly, there were similar proportions of CD8$^+$ TIL subsets between the two subgroups (Supplementary Fig. S3).

We next performed PCA on cluster-level pseudobulk gene expression profiles of tumor samples. CD8$^+$ TILs from *KRAS*^{mut}/*STK11*^{mut} tumors were markedly transcriptionally distinct from CD8$^+$ TILs from *KRAS*^{mut}/*STK11*^{wt} tumors (canonical correlation = 0.935, $P <$ 1e–4; **Fig. 2D**).

CD8$^+$ TILs from co-mutated tumors exhibit features of terminal dysfunction

To identify distinct transcriptional programs based on co-mutation status, we performed differential gene expression analyses on all CD8$^+$ TILs using SAVER-imputed expression values (20). Paradoxically, despite their clinically inferior response to neoadjuvant ICB, we found that CD8$^+$ TILs from *KRAS*^{mut}/*STK11*^{mut} tumors were enriched in multiple molecules canonically associated with effector function, specifically *GNLY*, *GZMA*, *PRF1*, *GZMB*, *GZMH*, *CCL5* (RANTES), and *NKG7* (**Fig. 3A** and **B**; Supplementary Table S4). However, more granular studies have identified a high degree of overlap between canonical markers of cytotoxic T cells and markers of T-cell dysfunction, or "exhaustion." *GZMA*, *GZMB*, *PRF1*, and *CCL5* when co-expressed with high levels of known T-cell checkpoints, such as *HAVCR2* (TIM-3) and *LAG3*, mark terminally dysfunctional CD8$^+$ TILs (21). Indeed, CD8$^+$ TILs from *KRAS*^{mut}/*STK11*^{mut} tumors more highly expressed checkpoints and molecules reflective of T-cell dysfunction (22), including *ENTPD1* (CD39), *HAVCR2* (TIM-3), *LAG3*, and *TOX*, as well as *TOX2* ($P <$ 2.22e–16 for all; **Fig. 3C–E**; Supplementary Fig. S4), which we have previously shown is highly expressed on tumor-reactive TILs from ICB-nonresponsive tumors (17), suggesting that this may be a more specific marker for dysfunctional tumor-reactive TILs than *TOX* (23, 24). Consistent with these findings, CD8$^+$ TILs from *KRAS*^{mut}/*STK11*^{mut} tumors had higher immune checkpoint (comprised of *PD-1*, *TIM-3*, *LAG3*, *CTLA4*, and *CD39*; $P <$ 2.22e–16) and cytotoxicity ($P <$ 2.22e–16) scores, whereas those from *KRAS*^{mut}/*STK11*^{wt} tumors had a higher memory score ($P <$ 2.22e–16; Supplementary Fig. S4; refs. 11, 15). *ITGAE* (CD103) and *ZNF683* (HOBIT), the canonical markers of tissue residence, were highly enriched in CD8$^+$ TILs from co-mutant tumors ($P <$ 2.22e–16 and $P <$ 2.22e–16, respectively; **Fig. 3F**), and CD63 was among the top differential genes in TILs from *KRAS*^{mut}/*STK11*^{mut} tumors, suggestive of a state of sustained T-cell activation associated with prolonged antigen exposure within the tumor in the absence of appropriate co-stimulatory signals that maintain productive function (**Fig. 3A**; Supplementary Table S4; ref. 25). Consistent with this notion, IL-7R, which maintains memory cell viability, is significantly more lowly expressed in TILs from *KRAS*^{mut}/*STK11*^{mut} tumors relative to TILs from *KRAS*^{mut}/*STK11*^{wt} tumors (**Fig. 3G**). These findings implicate a more dysfunctional T-cell phenotype associated with chronic antigen stimulation in *KRAS*^{mut}/*STK11*^{mut} tumors.

PGE2 signaling pathways are upregulated in CD8$^+$ TILs from KRAS^{mut}/STK11^{wt} tumors

In contrast, CD8$^+$ TILs from *KRAS*^{mut}/*STK11*^{wt} tumors were enriched in *NR4A3* (**Fig. 3A** and **B**; Supplementary Table S4), a transcription factor that is routinely associated with differentiation of short-lived effector cells (26–28), is upregulated within 1 to 3 hours after TCR stimulation (29), and, notably, has been shown to bind prostaglandins (30). Consistent with the upregulation of *NR4A3*, several additional genes associated with prostaglandin signaling were among the top differentially expressed genes in CD8$^+$ TIL from *STK11*^{wt} tumors, including *TENT5C*, *CREM*, and *FOSL2* (**Fig. 3A** and **B**; Supplementary Table S4; ref. 31). *PTGER4*, which encodes the PGE2 receptor EP4 and has been extensively shown to initiate T-cell immunosuppression, was also among these genes. The higher *PTGER4* expression in the *KRAS*^{mut}/*STK11*^{wt} cohort was consistent across patients (**Fig. 3H**). Expression of *PTGER2*, another immunosuppressive PGE2 receptor, was significantly higher in TILs from *KRAS*^{mut}/*STK11*^{wt} tumors (**Fig. 3H**; $P <$ 2.22e–16). Absolute expression of the immunostimulatory PGE2 receptors *PTGER1* and *PTGER3* in both cohorts was very low (Supplementary Fig. S4). To further support an increase in PGE2 signaling in CD8$^+$ TILs from *KRAS*^{mut}/*STK11*^{wt} tumors, *PDE7A*, an intracellular messenger for PGE2, was also upregulated (Supplementary Fig. S4; $P <$ 2.22e–16), as were *SYTL3* and *DDIT4*, which were both highly upregulated in T cells stimulated *ex vivo* with PGE2 ($P <$ 2.22e–16 for both; ref. 31).

Owing to the highly paradoxical nature of the observation that patients with *KRAS*^{mut}/*STK11*^{wt} tumors (i.e., more favorable clinical outcome) had evidence of more PGE2 signaling in CD8$^+$ TILs, we queried molecules downstream of PGE2 signaling in single-cell TCR-seq/RNA-seq data from our previously published cohort of *KRAS*^{wt} lung cancers treated with neoadjuvant PD-1 blockade (11) and indeed detected higher levels of *CREM*, *FOSL2*, *PTGER4*, and *NR4A3* in patients that did not have disease recurrence ($P <$ 2.22e–16 for all; Supplementary Fig. S5), suggesting that PGE2 signaling pathways in CD8$^+$ TILs may actually be beneficial for the immunotherapy response in general.

Work by Villa and colleagues (32) showed that signaling through EP4 initiates mitophagy, resulting in reduced mitochondrial mass, membrane potential, metabolic fitness, and, consequently, T-cell longevity. We therefore hypothesized that the reduction in mitochondrial mass associated with EP4 signaling would be accompanied by reduced OXPHOS in TILs from *KRAS*^{mut}/*STK11*^{wt} tumors. Indeed, expression of an OXPHOS gene signature (16) was downregulated (**Fig. 3I** and **J**; Supplementary Fig. S6; $P <$ 2.22e−16). This OXPHOS signature was also higher in tumors relative to the adjacent normal lung from the same patients in our *KRAS*^{mut}/*STK11*^{mut} ($P <$ 2.22e–16) and *KRAS*^{mut}/*STK11*^{wt} ($P <$ 2.22e–16) cohorts (Supplementary Fig. S4).

PGE2 is also known to dampen intratumoral T-cell responses via IL-2 receptor γ chain (*IL-2RG*) downregulation, thus reducing IL-2 signaling, but it does not affect the priming of new T cells in tumor-draining lymph nodes (31, 33). Indeed, the increase in genes associated with PGE2 signaling in TILs from *KRAS*^{mut}/*STK11*^{wt} tumors was accompanied by reduced expression of both IL-2RG ($P <$ 2.22e–16) and a gene set associated with IL-2 signaling ($P <$ 2.22e–16; **Fig. 3K** and **L**). Further supporting this notion, *SOCS1*, a negative

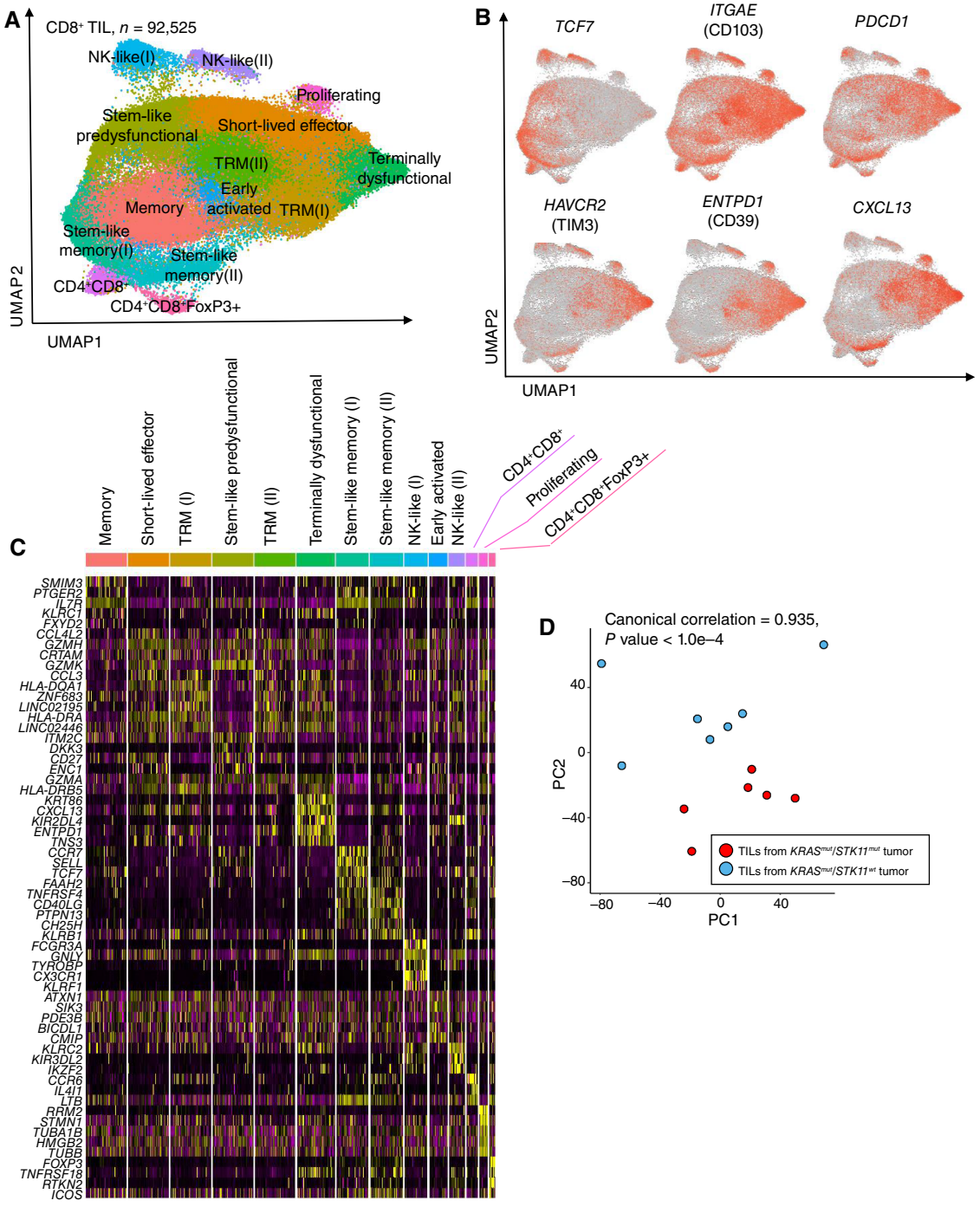

Figure 2.

Transcriptional profiling of neoadjuvant ICB-treated CD8$^+$ TILs in NSCLC based on *KRAS* and *STK11* co-mutation status. **A,** Refined clustering was performed on 92,525 CD8$^+$ T cells from tumor ($n = 13$), normal adjacent the lung ($n = 7$) and the previously published tissues for MD043-011, which includes tumor-draining lymph node and a distant brain metastasis. Fourteen distinct clusters were annotated and are marked by color on the Uniform Manifold Approximation and Projection (UMAP) projection. **B,** Expression of memory, TRM, and T-cell checkpoint markers, including *CXCL13* and *CD39*. **C,** Relative expression of the top five most differentially expressed genes. Five thousand cells were randomly sampled from each cluster for visualization. **D,** PCA of cell cluster–level pseudobulk gene expression for individual tumor samples ($n = 13$), based on co-mutation status. A one-sided permutation test was performed.

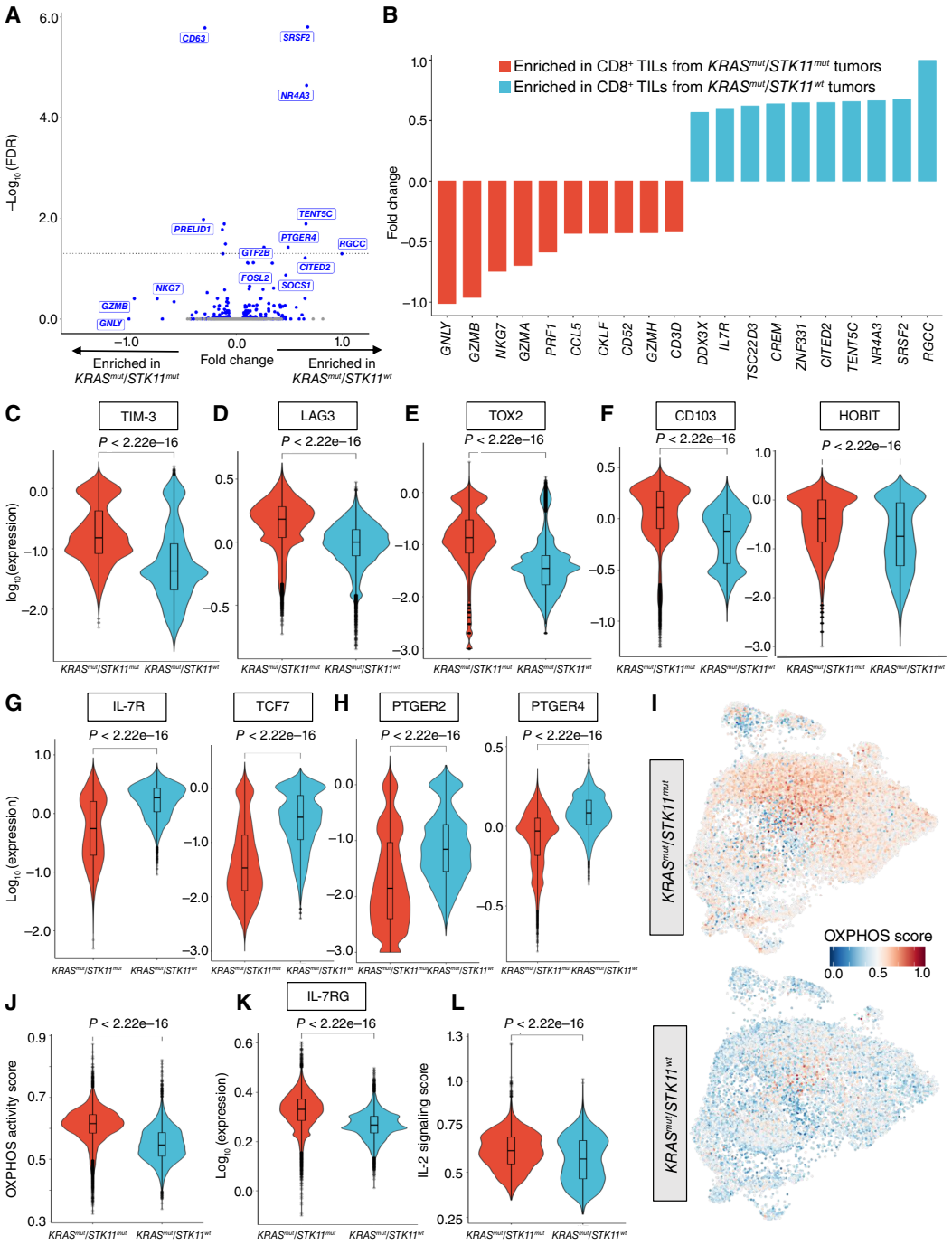

Figure 3.

CD8$^+$ TILs from co-mutated lung cancers exhibit features consistent with terminal differentiation and metabolic dysfunction. **A,** Volcano plot showing differential expression of CD8$^+$ TILs between *KRAS*^{mut}/*STK11*^{mut} tumors (left) and *KRAS*^{mut}/*STK11*^{wt} tumors (right). Each dot represents one gene. A FDR <0.05 was considered significant. **B,** A waterfall plot of the top 10 significantly upregulated genes enriched in *KRAS*^{mut}/*STK11*^{mut} (red) and in *KRAS*^{mut}/*STK11*^{wt} (blue) CD8$^+$ TILs. **C–E,** Violin plots for the expression of TIM-3, LAG3, and TOX2 in CD8$^+$ TILs between *KRAS*^{mut}/*STK11*^{mut} (red) and *KRAS*^{mut}/*STK11*^{wt} (blue) tumors. Comparisons were performed at the individual cell level using the two-sided Wilcoxon rank-sum test. **F–H,** Violin plots for the expression of key genes associated with tissue residence, memory, and prostaglandin receptor markers, in CD8$^+$ TILs between *KRAS*^{mut}/*STK11*^{mut} (red) and *KRAS*^{mut}/*STK11*^{wt} (blue) tumors. Comparisons were performed at the individual cell level using the two-sided Wilcoxon rank-sum test. **I,** Feature plot for the OXPHOS score on CD8$^+$ TILs from *KRAS*^{mut}/*STK11*^{mut} (top) and *KRAS*^{mut}/*STK11*^{wt} (bottom) tumor resections. This score ranges from 0–1. **J,** Violin plot of the OXPHOS score in CD8$^+$ TILs based on co-mutation status; a two-sided Wilcoxon rank-sum test was performed. **K,** Violin plot of the expression of IL-2RG in CD8$^+$ TILs between *KRAS*^{mut}/*STK11*^{mut} (red) and *KRAS*^{mut}/*STK11*^{wt} (blue) tumors. Comparisons were performed at the individual cell level using the two-sided Wilcoxon rank-sum test. **L,** Violin plot of the IL-2 signaling in CD8$^+$ TILs based on co-mutation status; a two-sided Wilcoxon rank-sum test was performed.

regulator of IL-2 signaling in T cells (34), and *RGCC*, which reduces IL-2 production and prevents cell-cycle activation (35), were upregulated in TILs from $KRAS^{mut}/STK11^{wt}$ tumors (**Fig. 3A** and **B**; Supplementary Table S4). These cells were also enriched in *IL-7R* expression ($P < 2.22e{-}16$), which in murine models is upregulated on antitumor memory cells that are critical in preventing tumor relapse after immunotherapy or surgical resection (36); *TCF7* ($P < 2.22e{-}16$), which is gradually downregulated with increasing T-cell dysfunction and decreased proliferative potential (**Fig. 3G**; ref. 37); *TBX21* (Tbet), a master transcriptional regulator of cytotoxic T-cell responses; and the short-lived effector molecule KLRG1 (Supplementary Fig. S4; $P < 2.22e{-}16$).

To further test if the differences in PGE2 and IL-2 signaling were specific to the $KRAS^{mut}/STK11^{mut}$ TME or if they were associated with relapse in general, we queried single-cell transcriptomic data from $KRAS^{wt}/STK11^{wt}$ lung tumors treated as part of the same neoadjuvant clinical trial. These data were published previously (11). Indeed, tumors that did not relapse had higher expression of several molecules associated with PGE2 signaling and suppression of IL-2 signaling, including CREM, FOSL2, NR4A3, TENT5C, RGCC, and PTGER4, and had a lower IL-2 signaling score (Supplementary Fig. S4). Together, and contrary to conventional view of PGE2 as broadly immune inhibitory, these findings suggest that in certain settings, such as neoadjuvant ICB treatment, increased expression of PGE2 signaling pathways and decreased expression of IL-2 signaling pathways in $CD8^+$ TILs from $KRAS^{mut}/STK11^{wt}$ tumors may enhance productive antitumor immunity.

Discussion

In the present study, we investigated the clinical and immunologic impacts of *STK11* mutations in resectable $KRAS^{mut}$ lung cancer treated with neoadjuvant ICB and uncovered an unexpected $CD8^+$ TIL biology associated with less favorable clinical outcomes in co-mutated cancers. In conjunction with the distinct clinical outcomes in our *KRAS*-mutant cohort, we observed a corresponding divergence in underlying $CD8^+$ T-cell transcriptional programs based on *STK11* co-mutation status. Our findings suggest that $KRAS^{mut}/STK11^{mut}$ $CD8^+$ TILs exhibit a terminally differentiated and dysfunctional phenotype, with high expression of *ENTPD1* (*CD39*), *TOX2*, and several T-cell checkpoints, in addition to classical cytotoxicity genes (*GZMA*, *GZMB*, *GZMH*, *NKG7*, and perforin). In contrast, molecules downstream of PGE2 signaling and inhibition of IL-2 signaling were notably enriched in $KRAS^{mut}/STK11^{wt}$ tumors.

Although stage IV $KRAS^{mut}/STK11^{mut}$ lung cancers are known to be less responsive to ICB than $KRAS^{mut}/STK11^{wt}$ lung cancers, the current study is one of the first to find that patients with $KRAS^{mut}/STK11^{mut}$ disease also had significantly higher risk of recurrence after neoadjuvant ICB and definitive resection. In this relatively limited sized cohort, there was not a statistical difference in the MPR rates between the two groups. This apparent discordance between pathologic response and RFS may be due to the threshold for "pathologic response" used in this trial (≤10% residual viable tumor). Indeed, when using an alternative pathologic cut-point of 50%, previously termed partial pathologic response in other solid tumor malignancies (18), there was a trend toward a higher rate of partial pathologic response in the $KRAS^{mut}/STK11^{wt}$ subgroup. Nonetheless, a key caveat in this relationship between pathologic response and long-term clinical outcomes is the assessment of nodal regression, which was not part of the pathologic response assessment in this protocol. Previous literature has described the additive prognostic value of combining both nodal and primary tumor regression statuses in terms of event-free survival (38). Taken together, despite evidence showing the prognostic value of pCR and MPR cut-points in this setting (39), the optimal pathologic regression threshold to predict clinical benefit may require further investigation, perhaps incorporating additional layers of clinicogenomic factors such as underlying molecular characteristics.

The striking differences in transcriptional programs between CD8 TILs from the $KRAS^{mut}/STK11^{mut}$ and $KRAS^{mut}/STK11^{wt}$ tumors seem at odds with an extensive body of literature supporting the T-cell inhibitory impacts of PGE2 signaling through the EP2 and EP4 receptors; however, this has not been studied in human biospecimens obtained after ICB. This is nonetheless perplexing, owing to a prior study showing increased levels of COX-2, which synthesizes PGE2 from arachidonic acid, in *STK11*-deficient lung cancers (40). It is possible that PGE2 signaling in $CD8^+$ TILs from $KRAS^{mut}/STK11^{wt}$ tumors promotes shorter survival, more rapid turnover, and overall reduced time in the chronically immunostimulatory, metabolically stressful TME. Indeed, our expression analyses of tissue residence markers support this hypothesis. It is also possible that $CD8^+$ TILs from $STK11^{mut}$ tumors are less sensitive to PGE2 as a result of biological or metabolic dysregulation in the $STK11^{mut}$ TME. Alternatively, the increase in expression of molecules associated with PGE2 signaling could reflect negative feedback inhibition in the $STK11^{mut}$ tumors; however, work by Villa and colleagues (32) shows that *PTGER4* expression increases upon encounter with PGE2, thus making this an unlikely explanation. Although we hypothesized that increased mitochondrial mass and lower PGE2 signaling could explain the higher levels of OXPHOS in TILs from $KRAS^{mut}/STK11^{mut}$ tumors, we cannot eliminate the possibility that this is instead resultant from metabolic disruption of the TME caused by the *STK11* mutation itself (41).

Accompanying these distinct transcriptional phenotypes, metabolic reprogramming of these T-cell populations was also described, whereby $CD8^+$ TILs from $KRAS^{mut}/STK11^{mut}$ tumors demonstrated high reliance on the OXPHOS pathway. This pattern of high OXPHOS $CD8^+$ TIL subsets has been previously associated with resistance to ICB in other clinical contexts (42). Previous work has also highlighted the increased energetic demands of $KRAS^{mut}/STK11^{mut}$ tumors; however, the impact of this on TILs as it relates to *KRAS/STK11* co-mutation is underexplored. Our work provides an intriguing first look into the metabolic disruption of T cells in the *STK11*-deficient TME. Given the appreciation that *STK11*-mutant tumors have a dependence on glutamine metabolism, current efforts are exploring the role of glutaminase inhibitors in both *STK11*-altered and *KEAP1*-altered NSCLC (NCT04250545). Our work, along with previously reported findings (41), suggests that this may be a rational strategy in *KRAS/STK11* co-mutated NSCLC in combination with ICB. With that said, it is surprising that the defining genes in TILs from $KRAS^{mut}/STK11^{mut}$ tumors were not directly related to metabolic dysfunction. In spite of the differences in OXPHOS, these genes were not among the top most differentially expressed. This raises the possibility that the combination of mutations in *KRAS* and *STK11* promotes downstream modulation of PGE2 and, consequently, IL-2 signaling in CD8 TILs that could negatively influence their ability to prevent or delay relapse.

Although preliminary, our exploratory findings suggest that T-cell turnover in the $KRAS^{mut}/STK11^{wt}$ TME may be beneficial for delaying or preventing relapse after neoadjuvant ICB and surgical resection. It may be that prolonged tumor residence prevents the formation of a highly proliferative stem-like compartment, which has been associated with favorable outcomes (21, 43, 44), whereas a

higher rate of T-cell turnover and, presumably, T-cell priming confers clinical benefit in the context of immunotherapy for lung cancer. Future studies should examine the specific impact of increased PGE2 signaling and decreased IL-2 signaling on T-cell turnover in the TME as it relates to checkpoint blockade response and clinical efficacy, regardless of *KRAS* or *STK11* mutation status. It may be that some aspect of the *KRAS*^{mut}/*STK11*^{mut} TME specifically amplifies inhibition of PGE2 signaling, which will be explored in future work. Consistent with this hypothesis, work by Best and colleagues (41) showed that efficient glutaminase metabolism, which we know is a critical component of *STK11*-deficient lung tumors, promotes activation-induced CD8$^+$ T-cell expansion. Thus, uncoupling T-cell "activation" from "dysfunction" and "exhaustion" in human cancer will help us better understand the mechanistic underpinnings of the observations presented here.

This study has important limitations to acknowledge, including the exploratory nature of this analysis, which is meant to provide a new hypothesis for future investigations. The small cohort size and heterogeneity in neoadjuvant treatment regimens limit our ability to draw definitive conclusions; however, the overall RFS signal from this cohort is encouraging. Additionally, limited availability of patient tissue samples, particularly from patients with *KRAS*^{wt}/*STK11*^{mut} disease, affects our ability to draw broad conclusions on the consequence of *STK11* mutation alone on T cells within the TME (45). Additionally, our study is unable to determine if the transcriptional differences between our genomic subgroups are inherent to their respective TME, or if they are the result of checkpoint blockade itself. Despite the limited sample size, we show a large effect size when comparing the transcriptomic differences according to co-mutation status, thus providing a robust foundation for future studies to expand on our initial findings. It is also worth noting that although we observed large differences in OXPHOS gene signatures between TILs from *KRAS*^{mut}/*STK11*^{wt} and *KRAS*^{mut}/*STK11*^{mut} tumors, detailed functional and mechanistic studies are needed to fully understand the functional impacts of these transcriptional differences.

In conclusion, and within the limitations of cohort size, we provide an initial analysis of clinical outcomes following neoadjuvant ICB for *KRAS*^{mut} NSCLC according to *STK11* co-mutation status and show evidence of global CD8$^+$ TIL disruption in those tumors harboring both mutations. These distinct functional features in *KRAS*^{mut}/*STK11*^{mut} CD8$^+$ TILs corresponded with higher recurrence risk, highlighting the increasing clinical need to offer more personalized perioperative strategies based on key genomic subgroups.

Authors' Disclosures

S. Rosner reports grants from Conquer Cancer/American Society of Clinical Oncology during the conduct of the study, as well as personal fees from MJH, EmPartners, Axiom, ASCO Advantage, Cardinal Health, Life Sciences FGI, Regeneron, and AstraZeneca outside the submitted work. J.E. Reuss reports personal fees from AstraZeneca, Bristol Myers Squibb, Arcus, AbbVie, Daiichi Sankyo, Catalym, Seagen, Gilead, Janssen, Novocure, Regeneron, Summit Therapeutics, and Pfizer and grants from Genentech, Verastem, Nuvalent, Exelixis, and Arcus outside the submitted work. S.R. Broderick reports other support from Bristol Myers Squibb and AstraZeneca outside the submitted work. D.R. Jones reports other support from AstraZeneca and grants from Merck outside the submitted work. J.S. Deutsch reports grants from Bristol Myers Squibb outside the submitted work, as well as a patent for PCT/US2023/013869 pending. J. Chaft reports grants from NCI P30 CA008748 Cancer Center Support Grant during the conduct of the study, as well as grants and personal fees from AstraZeneca, Merck, and Genentech/Roche, grants from Bristol Myers Squibb and BeiGene, and personal fees from Guardant Health, Boehringer Ingelheim, Janssen, Eli Lilly and Company, and Sanofi-Regeneron outside the submitted work. J. Spicer reports grants, personal fees, and nonfinancial support from Bristol Myers Squibb, Merck, and AstraZeneca, grants from CLS Therapeutics, and personal fees from Roche, Daiichi Sankyo, Regeneron, Eisai, Pfizer, and Amgen outside the submitted work. J. Taube reports grants and other support from Bristol Myers Squibb, other support from AstraZeneca, Elephas, Regeneron, Merck & Co, and Lunaphore, and grants, nonfinancial support, and other support from Akoya Biosciences outside the submitted work. V. Anagnostou reports grants from AstraZeneca, Bristol Myers Squibb, Delfi Diagnostics, and Personal Genome Diagnostics and personal fees from NeoGenomics, AstraZeneca, Foundation Medicine, and Personal Genome Diagnostics outside the submitted work, as well as a patent for Cancer Genomic Analyses, ctDNA Therapeutic Response Monitoring and Immunogenomic Features of Response to Immunotherapy (63/276,525; 17/779,936; 16/312,152; 16/341,862; 17/047,006; 17/598,690) issued. J.R. Brahmer reports grants and personal fees from Bristol Myers Squibb during the conduct of the study, as well as grants and personal fees from AstraZeneca and personal fees from Summit Therapeutics and Amgen outside the submitted work. D.M. Pardoll reports grants from Bristol Myers Squibb during the conduct of the study, as well as a patent for LAG3 Blockade in Cancer Therapy PCT/US04/006133 (as well as national-stage filings, continuations, and divisional applications therefrom; JHU Ref. C04255) issued to Bristol Myers Squibb. H. Ji reports grants from NIH during the conduct of the study, as well as grants from NIH outside the submitted work. P.M. Forde reports grants from Bristol Myers Squibb during the conduct of the study as well as grants and personal fees from AstraZeneca, Bristol Myers Squibb, Novartis, Regeneron, and BioNTech and receiving consulting fees from Ascendis, AstraZeneca, Bristol Myers Squibb, CureVac, Novartis, Regeneron, G1, Genlux, Genentech, Gritstones, Merck, Janssen, F-star, Sanofi, Amgen, Fosun, Teva, Synthekine, Flame, iTeos, and Tavotek outside the submitted work. K.A. Marrone reports grants, personal fees, and nonfinancial support from Bristol Myers Squibb, personal fees and nonfinancial support from Mirati Therapeutics, and personal fees from Regeneron, Janssen, Daiichi Sankyo, Amgen, AstraZeneca, and Merus outside the submitted work. K.N. Smith reports grants from Bristol Myers Squibb during the conduct of the study; grants from AbbVie and Bristol Myers Squibb outside the submitted work; a patent for MANAFEST Technology licensed and with royalties paid from Clasp Therapeutics and a patent for TCRs Targeting Mutated Oncogenes pending; and being a Scientific Founder with stock options in Clasp Therapeutics. No disclosures were reported by the other authors.

Authors' Contributions

S. Rosner: Conceptualization, resources, data curation, formal analysis, supervision, investigation, visualization, methodology, writing–original draft, project administration, writing–review and editing. **S. Connor:** Conceptualization, resources, data curation, software, formal analysis, validation, investigation, visualization, methodology, writing–original draft, writing–review and editing. **K. Sanber:** Conceptualization, supervision, methodology, writing–original draft. **M. Zahurak:** Software, formal analysis, methodology. **T. Zhang:** Resources, formal analysis. **I. Gurumurthy:** Formal analysis. **Z. Zeng:** Formal analysis. **B. Presson:** Formal analysis. **D. Singh:** Resources, formal analysis. **R. Rayes:** Data curation. **L. Sivapalan:** Resources, data curation, formal analysis. **G. Pereira:** Resources, data curation. **Z. Ji:** Data curation, formal analysis. **R. Thummalapalli:** Data curation. **J.E. Reuss:** Data curation, formal analysis, investigation, writing–review and editing. **S.R. Broderick:** Data curation, investigation. **D.R. Jones:** Data curation, investigation. **J.S. Deutsch:** Data curation, formal analysis, supervision, investigation, methodology, writing–review and editing. **T.R. Cottrell:** Data curation, formal analysis, supervision. **J. Chaft:** Data curation, formal analysis, supervision, funding acquisition, investigation. **J. Spicer:** Resources, supervision, investigation, writing–review and editing. **J. Taube:** Formal analysis, supervision, investigation. **V. Anagnostou:** Resources, formal analysis, supervision, investigation, methodology, writing–review and editing. **J.R. Brahmer:** Supervision, investigation, writing–review and editing. **D.M. Pardoll:** Conceptualization, formal analysis, supervision, methodology, writing–original draft, writing–review and editing. **H. Ji:** Conceptualization, software, formal analysis, supervision, validation, investigation, methodology, writing–review and editing. **P.M. Forde:** Conceptualization, resources, formal analysis, supervision, investigation, methodology, writing–original draft, writing–review and editing. **K.A. Marrone:** Conceptualization, resources, formal analysis, supervision, funding acquisition, investigation, methodology, writing–original draft, writing–review and editing. **K.N. Smith:** Conceptualization, resources, data curation, software, formal analysis, supervision, funding acquisition, validation, investigation, visualization, methodology, writing–original draft, writing–review and editing.

Acknowledgments

This work was supported by the LUNGevity Foundation, the Lung Cancer Foundation of America, Swim Across America, The Mark Foundation for Cancer Research, The Bloomberg~Kimmel Institute for Cancer Immunotherapy, Conquer Cancer, Bristol Myers Squibb, the American Lung Association, the Commonwealth Foundation, and NIH grants R37 CA251447, CCSG P30 CA008748, and P30 CA006973.

Note

Supplementary data for this article are available at Clinical Cancer Research Online (http://clincancerres.aacrjournals.org/).

Received September 18, 2024; revised November 8, 2024; accepted November 13, 2024; published first November 15, 2024.

References

1. Sanber K, Rosner S, Forde PM, Marrone KA. Neoadjuvant immunotherapy for non-small cell lung cancer. BioDrugs 2023;37:775–91.
2. Forde PM, Spicer J, Lu S, Provencio M, Mitsudomi T, Awad MM, et al. Neoadjuvant nivolumab plus chemotherapy in resectable lung cancer. N Engl J Med 2022;386:1973–85.
3. Wakelee H, Liberman M, Kato T, Tsuboi M, Lee SH, Gao S, et al. Perioperative pembrolizumab for early-stage non–small-cell lung cancer. N Engl J Med 2023;389:491–503.
4. Cottrell TR, Thompson ED, Forde PM, Stein JE, Duffield AS, Anagnostou V, et al. Pathologic features of response to neoadjuvant anti-PD-1 in resected non-small-cell lung carcinoma: a proposal for quantitative immune-related pathologic response criteria (irPRC). Ann Oncol 2018;29:1853–60.
5. Rosner S, Liu C, Forde PM, Hu C. Association of pathologic complete response and long-term survival outcomes among patients treated with neoadjuvant chemotherapy or chemoradiotherapy for NSCLC: a meta-analysis. JTO Clin Res Rep 2022;3:100384.
6. Negrao MV, Skoulidis F, Montesion M, Schulze K, Bara I, Shen V, et al. Oncogene-specific differences in tumor mutational burden, PD-L1 expression, and outcomes from immunotherapy in non-small cell lung cancer. J Immunother Cancer 2021;9:e002891.
7. Judd J, Abdel Karim N, Khan H, Naqash AR, Baca Y, Xiu J, et al. Characterization of KRAS mutation subtypes in non–small cell lung cancer. Mol Cancer Ther 2021;20:2577–84.
8. Doroshow DB, Bhalla S, Beasley MB, Sholl LM, Kerr KM, Gnjatic S, et al. PD-L1 as a biomarker of response to immune-checkpoint inhibitors. Nat Rev Clin Oncol 2021;18:345–62.
9. Vokes NI, Liu D, Ricciuti B, Jimenez-Aguilar E, Rizvi H, Dietlein F, et al. Harmonization of tumor mutational burden quantification and association with response to immune checkpoint blockade in non-small-cell lung cancer. JCO Precis Oncol 2019;3:PO.19.00171.
10. Skoulidis F, Goldberg ME, Greenawalt DM, Hellmann MD, Awad MM, Gainor JF, et al. STK11/LKB1 mutations and PD-1 inhibitor resistance in KRAS-mutant lung adenocarcinoma. Cancer Discov 2018;8:822–35.
11. Caushi JX, Zhang J, Ji Z, Vaghasia A, Zhang B, Hsiue EHC, et al. Transcriptional programs of neoantigen-specific TIL in anti-PD-1-treated lung cancers. Nature 2021;596:126–32.
12. Forde PM, Chaft JE, Smith KN, Anagnostou V, Cottrell TR, Hellmann MD, et al. Neoadjuvant PD-1 blockade in resectable lung cancer. N Engl J Med 2018;378:1976–86.
13. Reuss JE, Anagnostou V, Cottrell TR, Smith KN, Verde F, Zahurak M, et al. Neoadjuvant nivolumab plus ipilimumab in resectable non-small cell lung cancer. J Immunother Cancer 2020;8:e001282.
14. Rosner S, Reuss JE, Zahurak M, Zhang J, Zeng Z, Taube J, et al. Five-year clinical outcomes after neoadjuvant nivolumab in resectable non–small cell lung cancer. Clin Cancer Res 2023;29:705–10.
15. Oliveira G, Egloff AM, Afeyan AB, Wolff JO, Zeng Z, Chernock RD, et al. Preexisting tumor-resident T cells with cytotoxic potential associate with response to neoadjuvant anti-PD-1 in head and neck cancer. Sci Immunol 2023;8:eadf4968.
16. Fernández-García J, Franco F, Parik S, Altea-Manzano P, Pane AA, Broekaert D, et al. $CD8^+$ T cell metabolic rewiring defined by scRNA-seq identifies a critical role of ASNS expression dynamics in T cell differentiation. Cell Rep 2022;41:111639.
17. Prior IA, Hood FE, Hartley JL. The frequency of ras mutations in cancer. Cancer Res 2020;80:2969–74.
18. Menzies AM, Amaria RN, Rozeman EA, Huang AC, Tetzlaff MT, van de Wiel BA, et al. Pathological response and survival with neoadjuvant therapy in melanoma: a pooled analysis from the International Neoadjuvant Melanoma Consortium (INMC). Nat Med 2021;27:301–9.
19. Lo Iacono M, Monica V, Righi L, Grosso F, Libener R, Vatrano S, et al. Targeted next-generation sequencing of cancer genes in advanced stage malignant pleural mesothelioma: a retrospective study. J Thorac Oncol 2015;10:492–9.
20. Huang M, Wang J, Torre E, Dueck H, Shaffer S, Bonasio R, et al. SAVER: gene expression recovery for single-cell RNA sequencing. Nat Methods 2018;15:539–42.
21. Miller BC, Sen DR, Al Abosy R, Bi K, Virkud YV, LaFleur MW, et al. Subsets of exhausted $CD8^+$ T cells differentially mediate tumor control and respond to checkpoint blockade. Nat Immunol 2019;20:326–36.
22. Koyama S, Akbay EA, Li YY, Aref AR, Skoulidis F, Herter-Sprie GS, et al. STK11/LKB1 deficiency promotes neutrophil recruitment and proinflammatory cytokine production to suppress T-cell activity in the lung tumor microenvironment. Cancer Res 2016;76:999–1008.
23. Khan O, Giles JR, Mcdonald S, Manne S, Ngiow SF, Patel KP, et al. TOX transcriptionally and epigenetically programs $CD8^+$ T cell exhaustion. Nature 2019;571:211–18.
24. Seo H, Chen J, González-Avalos E, Samaniego-Castruita D, Das A, Wang YH, et al. TOX and TOX2 transcription factors cooperate with NR4A transcription factors to impose CD8 + T cell exhaustion. Proc Natl Acad Sci U S A 2019;116:12410–5.
25. Pfistershammer K, Majdic O, StöCkl J, Zlabinger G, Kirchberger S, Steinberger P, et al. CD63 as an activation-linked T cell costimulatory element. J Immunol 2004;173:6000–8.
26. Mackay LK, Rahimpour A, Ma JZ, Collins N, Stock AT, Hafon ML, et al. The developmental pathway for $CD103^+CD8^+$ tissue-resident memory T cells of skin. Nat Immunol 2013;14:1294–301.
27. Beura LK, Wijeyesinghe S, Thompson EA, Macchietto MG, Rosato PC, Pierson MJ, et al. T cells in nonlymphoid tissues give rise to lymph-node-resident memory T cells. Immunity 2018;48:327–38.e5.
28. Kurd NS, He Z, Louis TL, Milner JJ, Omilusik KD, Jin W, et al. Early precursors and molecular determinants of tissue-resident memory $CD8^+$ T lymphocytes revealed by single-cell RNA sequencing. Sci Immunol 2020;5:eaaz6894.
29. Richard AC, Lun ATL, Lau WWY, Göttgens B, Marioni JC, Griffiths GM. T cell cytolytic capacity is independent of initial stimulation strength. Nat Immunol 2018;19:849–58.
30. Kagaya S, Ohkura N, Tsukada T, Miyagawa M, Sugita Y, Tsujimoto G, et al. Prostaglandin A2 acts as a transactivator for NOR1 (NR4A3) within the nuclear receptor superfamily. Biol Pharm Bull 2005;28:1603–7.
31. Morotti M, Grimm AJ, Hope HC, Arnaud M, Desbuisson M, Rayroux N, et al. PGE_2 inhibits TIL expansion by disrupting IL-2 signalling and mitochondrial function. Nature 2024;629:426–34.
32. Kishton RJ, Sukumar M, Restifo NP. Metabolic regulation of T cell longevity and function in tumor immunotherapy. Cell Metab 2017;26:94–109.
33. Lacher SB, Dörr J, De Almeida GP, Hönninger J, Bayerl F, Hirschberger A, et al. PGE_2 limits effector expansion of tumour-infiltrating stem-like $CD8^+$ T cells. Nature 2024;629:417–25.
34. Schlabach MR, Lin S, Collester ZR, Wrocklage C, Shenker S, Calnan C, et al. Rational design of a SOCS1-edited tumor-infiltrating lymphocyte therapy using CRISPR/Cas9 screens. J Clin Invest 2023;133:e163096.
35. Tegla CA, Cudrici CD, Nguyen V, Danoff J, Kruszewski AM, Boodhoo D, et al. RGC-32 is a novel regulator of the T-lymphocyte cell cycle. Exp Mol Pathol 2015;98:328–37.
36. Micevic G, Daniels A, Flem-Karlsen K, Park K, Talty R, McGeary M, et al. IL-7R licenses a population of epigenetically poised memory $CD8^+$ T cells with superior antitumor efficacy that are critical for melanoma memory. Proc Natl Acad Sci U S A 2023;120:e2304319120.
37. Van Der Leun AM, Thommen DS, Schumacher TN. $CD8^+$ T cell states in human cancer: insights from single-cell analysis. Nat Rev Cancer 2020;20:218–32.
38. Deutsch JS, Cimino-Mathews A, Thompson E, Provencio M, Forde PM, Spicer J, et al. Association between pathologic response and survival after neoadjuvant therapy in lung cancer. Nat Med 2024;30:218–28.
39. Hines JB, Cameron RB, Esposito A, Kim L, Porcu L, Nuccio A, et al. Evaluation of major pathologic response and pathologic complete response as surrogate end points for survival in randomized controlled trials of

neoadjuvant immune checkpoint blockade in resectable in NSCLC. J Thorac Oncol 2024;19:1108–16.
40. Cao C, Gao R, Zhang M, Amelio AL, Fallahi M, Chen Z, et al. Role of LKB1-CRTC1 on glycosylated COX-2 and response to COX-2 inhibition in lung cancer. J Natl Cancer Inst 2015;107:358.
41. Best SA, Gubser PM, Sethumadhavan S, Kersbergen A, Negrón Abril YL, Goldford J, et al. Glutaminase inhibition impairs CD8 T cell activation in STK11-/Lkb1-deficient lung cancer. Cell Metab 2022;34:874–87.e6.
42. Li C, Phoon YP, Karlinsey K, Tian YF, Thapaliya S, Thongkum A, et al. A high OXPHOS CD8 T cell subset is predictive of immunotherapy resistance in melanoma patients. J Exp Med 2022;219:e20202084.
43. Siddiqui I, Schaeuble K, Chennupati V, Fuertes Marraco SA, Calderon-Copete S, Pais Ferreira D, et al. Intratumoral Tcf1^{+}PD-1^{+}CD8^{+} T cells with stem-like properties promote tumor control in response to vaccination and checkpoint blockade immunotherapy. Immunity 2019;50:195–211.e10.
44. Sade-Feldman M, Yizhak K, Bjorgaard SL, Ray JP, de Boer CG, Jenkins RW, et al. Defining T cell states associated with response to checkpoint immunotherapy in melanoma. Cell 2018;175:998–1013.e20.
45. Li A, Wang Y, Yu Z, Tan Z, He L, Fu S, et al. STK11/LKB1-Deficient phenotype rather than mutation diminishes immunotherapy efficacy and represents STING/type I interferon/CD8^{+} T-cell dysfunction in NSCLC. J Thorac Oncol 2023;18:1714–30.